Research Square

Preprints are preliminary reports that have not undergone peer review.
They should not be considered conclusive, used to inform clinical practice,
or referenced by the media as validated information.

Identification of the First Highly Selective Inhibitor of Human Lactate Dehydrogenase B

sachio shibata (sachio.shibata@axcelead.com)
Axcelead Drug Discovery Partners, Inc. https://orcid.org/0000-0002-0347-1911

Satoshi Sogabe
Axcelead Drug Discovery Partners, Inc.

Masanori Miwa
Axcelead Drug Discovery Partners, Inc.

Takuya Fujimoto
Axcelead Drug Discovery Partners, Inc.

Nobuyuki Takakura
Axcelead Drug Discovery Partners, Inc.

Akihiko Naotsuka
Axcelead Drug Discovery Partners, Inc.

Shuji Kitamura
Axcelead Drug Discovery Partners, Inc.

Tomohiro Kawamoto
Axcelead Drug Discovery Partners, Inc.

Tomoyoshi Soga
Keio University

Article

Keywords: Lactate dehydrogenase (LDH), LDHB

Posted Date: November 9th, 2020

DOI: https://doi.org/10.21203/rs.3.rs-95794/v1

License: This work is licensed under a Creative Commons Attribution 4.0 International License.
Read Full License

Loading [MathJax]/jax/output/CommonHTML/fonts/TeX/fontdata.js

Abstract

Lactate dehydrogenase (LDH) catalyses the conversion of pyruvate to lactate and NADH to NAD^+ and has two isoforms, LDHA and LDHB. LDHA is a promising target for cancer therapy, whereas LDHB is necessary for basal autophagy and cancer cell proliferation in oxidative and glycolytic cancer cells. To our knowledge, selective inhibitors for LDHB have yet to be reported. Here, we developed a high-throughput mass spectrometry screening system using an LDHB enzyme assay by detecting NADH and NAD^+. The screening campaign identified a small-molecule LDHB selective inhibitor AXKO-0046, an indole derivative. It exhibited uncompetitive LDHB inhibition (IC_{50} = 42 nM). X-ray crystallography identified its binding with the potential allosteric site away from the LDHB catalytic active site, suggesting that targeting the tetramerization interface of the two dimers is critical for enzymatic activity. AXKO-0046 and its derivatives can be used to validate LDHB-associated pathways in cancer metabolism.

Introduction

Cancer cells can reprogram various genes to promote their rapid proliferation and metastatic potentials. Unlike most normal cells, cancer cells can adapt to various microenvironments, such as hypoxia, depletion of glucose and other nutrients, and acidosis. Moreover, in tumours and other proliferating or developing cells, a metabolic switch known from normal oxidative phosphorylation to aerobic glycolysis is common. This adaptation known as the Warburg effect allows cancer cells to produce ATP from glucose by promoting glycolysis to produce lactate from the mitochondrial pyruvate pool, even in the presence of oxygen[1, 2]. Increased aerobic glycolysis provides cancer cells with a growth advantage despite its energetic inefficiency compared with anaerobic glycolysis[3].

During aerobic glycolysis, the conversion of pyruvate into lactate is mediated by cytosolic lactate dehydrogenase (LDH) enzymes with nicotinamide adenine dinucleotide (NADH) as a co-factor, which is converted to nicotinamide adenine dinucleotide (NAD^+). LDH enzymes are tetrameric enzymes comprising two separate subunits LDHA and LDHB and can form five isozymes, namely A4, A3B1, A2B2, A1B3, and B4, that correspond to five isoforms LDH5 to LDH1, respectively[4].

Previous studies have reported that LDHA (LDH5) plays a critical role in cancer. For instance, in gastric and non-small-cell lung cancer patients high LDHA levels have been correlated with tumour size and poor prognosis[5, 6]. In addition, LDHA silencing by siRNA or shRNA inhibited cell growth and tumorigenic potential both *in vitro* and in xenograft models[7, 8]. Therefore, several LDHA inhibitors have been developed whose hit target compounds have been identified through high-throughput screening (HTS)[9].

Meanwhile, LDHB (LDH1) has been associated with aggressive cancer phenotypes[10, 11]. One study used clinical samples derived from colorectal cancer patients and found that *MYC* expression highly correlated with those of various metabolic genes. In that study, 231 unique metabolic genes were identified and it was reported that LDHB levels were upregulated in colorectal cancer, whereas LDHA levels remained

Loading [MathJax]/jax/output/CommonHTML/fonts/TeX/fontdata.js

unchanged[12]. Furthermore, LDHB is a key contributor in lysosomal activity and autophagy in cancer[13]. Since many cancer cells upregulate autophagy, which is required to support metabolism, tumourigenesis, and resistance to therapy[14], it suggests that inhibition of LDHB could be a way forwards for the effective targeting. Moreover, LDHB was differentially expressed in triple-negative breast cancers that are defined by the absence of detectable estrogen receptor (*ER*) and progesterone receptor (*PR*) expression and the lack of human epidermal growth factor 2 (*HER2*) gene amplification[11]. *LDHB* knockdown selectively reduced the proliferation of breast cancer cells both *in vitro* and *in vivo*[11]. Triple-negative breast cancer cells exhibited enhanced glycolysis and utilise LDHB as an energy source. Therefore, we hypothesised that the inhibition of LDHB may be a promising therapeutic approach for targeting cancer metabolism.

Despite the suggested association between LDHB and cancer metabolism, LDHB selective inhibitors remain unexplored. In this study, to explore the selective LDHB inhibitors we developed a screening system to monitor the conversion of NADH to NDH^+ by LDHB using RapidFire-Mass (RF-MS) system. This assay system was robust and avoided false-positive results. We then identified that AXKO-0046, an indole derivative, selectively inhibited LDHB activity in an uncompetitive manner with respect to NADH and pyruvate. Moreover, structural analysis showed that AXKO-0046 does not bind in the catalytic site of the enzyme but significantly binds to LDHB in the novel allosteric site of the tetramer. The allosteric site is unique to LDHB based on sequence alignment, resulting in LDHB-selective inhibition. Taken together, our findings suggest that AXKO-0046 is a promising chemical probe to elucidate the roll of LDHB-associated pathways in cancer metabolism.

Results

Development and Optimization of RapidFire-Mass (RF-MS) for LDHB Activity

To identify small-molecule LDHB inhibitors, we developed an assay system in a 384-well format to measure LDHB activity through NADH and NAD^+ using RF-MS (Fig. 1a). The integrated peak areas were linear for concentrations of the NADH or NAD^+ standard between 1 and 100 μM (Supplementary Fig. 1). The extracted ion chromatogram of NADH also showed a NAD^+ fragment originating from the in-source decay (ISD) of NADH during ionization. Because the ISD of NAD^+ observed with NADH was less than 10% of the peak area of NADH, there was no contribution against the detection for LDHB activity.

Next, we optimised the assay conditions in RF-MS. Titration of human LDHB was examined at concentrations ranging from 0.0625 nM to 1 nM. Supplementary Fig. 2 shows a linear relationship between the velocity and enzyme concentration (0.0625–0.5 nM). We used a 0.25 nM LDHB throughout assay development and screening to ensure enzyme activation. Next, the concentrations of NADH and pyruvate were optimised. The Km values of NADH and pyruvate were 64 μM and 116 μM, respectively, in the presence of 500 μM pyruvate (Supplementary Fig. 2), The Km values obtained from the two assays [illegible] ased on the Km of each substrate and the

Loading [MathJax]/jax/output/CommonHTML/fonts/TeX/fontdata.js

robustness of the assay signal, NADH and pyruvate concentrations were both set at 75 μM for the screening.

High-throughput Screening Of Ldhb Inhibitors Using Rf-ms Assay

The screening campaign was performed on an in-house pooled diverse library of more than 345,000 compounds at a concentration of 10 μM as shown in the workflow (Fig. 1b). Assay quality was acceptable because Z' factors exceeded 0.65 and a signal-to-noise ratio greater than 5.0 was obtained (Fig. 1c). The hit rate was 0.22% when the threshold was set at ≥ 30% of inhibition compared with the control (Fig. 1d).

To identify the hit compounds in pooled samples, deconvolution assay was conducted at 30 μM compound concentration. Compounds containing oxalate salt, which has an inhibitory activity for LDH, were excluded, as they are undesirable inhibitors. Thus, 22 compounds showed activity with ≥30% inhibition rate and ≥80% purity corresponding to a hit rate of 0.006%. Subsequent dose–response experiments determined the IC_{50} values for all identified hit compounds.

Comparison of IC_{50} Values of hit compounds for LDHB and LDHA

To compare the selectivity potencies of the 22 selected compounds, we evaluated them against human LDHB and LDHA using RF-MS. To obtain comparable IC_{50} values, the substrate concentration was fixed to each Km determined using our assay conditions for each substrate pair. For LDHA, time-dependent accumulation of NADH was confirmed in a protein concentration-dependent manner (Supplementary Fig. 2). The Km value was also determined for the LDHA reaction. All IC_{50} values are listed in Supplementary Table 1.

Four compounds (i.e., AXKO-0004, AXKO-0008, AXKO-0010, and AXKO-0013) were observed to exhibit significant differences in potency (IC_{50}) between LDHB and LDHA. Although AXKO-010 was a partial inhibitor at the highest compound concentration, this was not due to compound concentration effects, such as aggregation, instability, or assay interference. It exhibited LDHB inhibitory activity with IC_{50} ≤3 μM and no inhibitory activity against LDHA at 300 μM, thus showing >100-fold selectivity over LDHA (Supplementary Table 1).

To find more potent compounds than AXKO-0010, we then assessed the inhibitory effects of 75 compounds of indole derivatives with as substructural similarity from the compound library. AXKO-0046 was identified as N-({3-[2-(benzylamino) ethyl]-1H-indol-2-yl} methyl) cycloheptanamine and achieved highly potent LDHB inhibitory activity (IC_{50} = 42 nM) with selectivity over LDHA (Fig. 2).

Characterization Of Axko-0046

Loading [MathJax]/jax/output/CommonHTML/fonts/TeX/fontdata.js

To understand the underlying inhibition mechanism, substrate competition assays were performed. LDHB inhibition activities for AXKO-0046 were assessed at different concentrations of the substrate. The inhibitory activity of AXKO-0046 increased dependent on the concentrations of NADH. Similar to NADH, AXKO-0046 exhibited decreasing IC_{50} values at increasing pyruvate concentrations, indicating that it was uncompetitive with both substrates (Fig. 3a and Supplementary Table 2).

Meanwhile, the Km and Vmax values for LDHB were determined in the presence AXKO-0046. As the AXKO-0046 concentration increased in the reactions, both Vmax and Km decreased proportionally (Supplementary Fig. 3 and Table 1). The Lineweaver – Burke plot lines were nearly parallel (Fig. 3b), indicating uncompetitive inhibition with a strong preference for inhibiting the enzyme – substrate complex.

Table 1
Effect of AXKO-0046 on Km and Vmax of NADH and pyruvate on LDHB enzyme activity.

		AXKO-0046 concentration [μM]							
		0.00001	0.0001	0.001	0.01	0.1	1	10	100
NADH	Vmax ($\mu M\ min^{-1}$)	10.1	10.7	9.7	8.3	6.0	2.9	2.1	2.2
	SD ±	0.1	0.8	0.8	0.7	0.5	0.1	0.1	0.1
	Km (μM)	100.4	116	93.5	78.4	52.5	24.6	17.6	19.3
	SD ±	20.5	17.4	15.7	15.3	10.7	2.3	2.1	3.0
Pyruvate	Vmax ($\mu M\ min^{-1}$)	7.3	6.9	6.5	6.6	4.3	2.0	1.6	1.6
	SD ±	0.9	0.7	0.9	0.8	0.7	0.2	0.1	0.1
	Km (μM)	60.3	58.3	50.5	55.2	33.2	12.6	11.9	10.2
	SD ±	19.1	15.7	18.8	16.6	16.3	6.4	5.3	4.3

Then, we assessed whether there was any time dependence to the onset of inhibition by varying the time for which AXKO-0046 and LDHB were preincubated before initiating the enzymatic reaction. Following pre-incubation with LDHB for 120 min, the inhibition position of AXKO-0046 did not increase with preincubation time (Supplementary Fig. 4).

Characterization Of Axko-0046 Derivatives

Loading [MathJax]/jax/output/CommonHTML/fonts/TeX/fontdata.js

To assess the structure-and-activity relationship (SAR) of AXKO-0046, its derivatives were synthesised, and their inhibitory activities were evaluated. Methyl scanning is a well-known systematic approach to determine interaction sites between small molecules and macromolecular targets, thus providing opportunities for structural modifications to improve potency[17]. The structure and inhibitory activity of each compound is listed in Fig. 4.

AXKO-0046 contains three hydrogen bond donors (HBD), NH group of indole, benzylamine, and cycloheptylamine group, which can interact with the counter amino acid residues of LDHB. The introduction of the methyl group to the benzylamino group (AXKO-0060) resulted in a modest loss of inhibitory activity (IC_{50} = 0.26 μM), whereas the addition of the methyl group at the cycloheptylamino group (AXKO-0077) resulted in marked loss of activity (IC_{50} = 6.3 μM). The incorporation of two methyl groups into both amino groups (AXKO-0058) simultaneously reduced the activity (IC_{50} = 8.3 μM). Lastly, methylation at the 1-position of indole (AXKO-0067) led to a significant loss of potency (IC_{50} > 100 μM).

Structural Analysis Of Axko-0046 With Ldhb

To investigate the binding site, we solved the two crystal structures of LDHB; the binary complex with the cofactor NADH and the quaternary complex with NADH using the substrate analogue oxamate and the inhibitor AXKO-0046 at 1.80 Å and 1.55 Å resolution, respectively (Fig. 5a and Supplementary Table 3). Both structures exhibited the α/β protein folding conserved in the LDHA and LDHB structures as previously reported[18]. There are two tetramers for the binary complex and one tetramer for the quaternary complex in the asymmetric unit, respectively. The average root-mean-square deviation (RMSD) values between the monomers in the asymmetric unit were 0.5 Å and 0.3 Å for two tetramers of binary complex and one tetramer of the quaternary complex, respectively. Electron density was visible for NADH and oxamate at the cofactor- and substrate-binding sites, respectively, whereas relatively weak but distinct electron density was visible for AXKO-0046 at the interface between the two monomers (Supplementary Fig. 5). These results indicated that the compound has alternative conformations on the 2-fold axis of the tetramer with relatively low occupancies.

The binding conformation of NADH with the enzyme is essentially identical between the binary complex and the quaternary complex, and their binding interactions were consistent with those of published structures. In the quaternary complex, oxamate is bound near the NADH nicotinamide moiety and interacts with the active-site loop (residues Glu101–Leu110), which is in a closed conformation. In contrast, in the binary complex, the active-site loops were partially disordered with an open conformation for the two tetramers in the asymmetric units, except for two of eight monomers in which the loop is well ordered due to crystal packing (Supplementary Fig. 6). The superimposition of our two structures clearly indicated structural changes corresponding to AXKO-0046 inhibition. Significant structural differences were observed around the active-site loop with a maximum RMSD of approximately 7 Å for the main-chain atoms. Other remarkable structural deviations, except for the active site, were observed in the two residues Asp311–Asp330) with a maximum

Loading [MathJax]/jax/output/CommonHTML/fonts/TeX/fontdata.js

RMSD of approximately 2 Å for backbone atoms (Supplementary Fig. 7). These structural variations are further discussed in the Discussion section to understand the inhibitory mechanism of AXKO-0046.

AXKO-0046 is located in an interfacial allosteric site between two monomers, approximately more than 20 Å away from the active site (Fig. 5b). Although the compound occupies the site with half-occupancy in the two possible orientations on a two-fold axis, only one orientation was defined due to the relatively poor electron density as described in Supplementary Fig. 5. The indole ring thus occupies in the small cavity composed of Gly204, Asn206, Gly209, and Ser211. In addition, the NH group of indole forms a hydrogen bond with the main-chain oxygen of Ser203. Two NH groups of benzylamine and cycloheptylamine interact with the side-chain oxygens of two Glu214 residues. The benzyl and the cycloheptyl groups are exposed to the solvent region and surrounded by Lys308 and Lys310, followed by the C-terminal helix with significant structural rearrangements, as described below.

Discussion

Many metabolic enzymes play a major role in cancer survival; however, they are not extensively exploited as drug targets. Therefore, in this study, we utilised LDHB as a drug target and developed an assay for high-throughput compound screening to identify LDHB inhibitors. To the best of our knowledge, LDHB specific inhibitors are unreported owing to the high structural homology between LDHB and LDHA, high structural homology of their catalytic site (89% according to the NCBI basic local alignment search tool [BLAST])[19]. Further, high-throughput screening for LDHB has not yet been previously conducted.

To date, *in vitro* LDH assays have been used to measure the fluorescence of NADH and has been previously reported to have a characteristic excitation maximum at 340 nm and an emission maximum at 480 nm[20]. However, this procedure can give rise to false positives and negatives because of fluorescence interference at the excitation and emission wavelengths of NADH. Although other methods, such as measuring NADH through the conversion of resazurin to resorufin by diaphorase using enzyme-coupled detection methods[9], have also been suggested, but inhibition of the coupling enzymes by test compounds may affect the assay and lead to false positives in HTS campaign.

Therefore, the Genentech group developed a label-free assay to monitor the conversion of pyruvate to lactate by LDHA using RF-MS[21]. However, it was only used for the secondary assay to confirm the selected compounds from initial screening employed fluorescence assay. In this study, instead of measuring the conversion from pyruvate to lactate, we established a robust RF-MS assay system to monitor that from NADH to NAD^+ using LDH activities. This method is useful not only for LDH but also for other dehydrogenases utilizing NADH or NAD^+. It also allowed us to conduct a HTS campaign using a large compound library. The assay showed excellent performance, having an average Z' factor ≥ 0.65 when more than 345,000 compounds were screened.

The hit rate of the screening campaign was very low at 0.006% with 30% inhibition threshold (Fig. 1d). This low hit rate was probably attributed to the fact that we screened against LDHA using a small compound

Loading [MathJax]/jax/output/CommonHTML/fonts/TeX/fontdata.js

library[21]. LDHA is considered a highly intractable target against a small molecule[16]. However, we found 22 substantially potent LDHB inhibitors, of which only 4 compounds (i.e., AXKO-0004, AXKO-0008, AXKO-0010, and AXKO-0013) showed high selectivity for LDHB after retesting at 5 doses. Among these hit compounds, AXKO-0010, with a central indole scaffold, showed excellent potency and selectivity as a LDHB inhibitor. However, it did not completely inhibit the enzyme activity even after its concentration was increased. Therefore, we next assessed the inhibitory effects of a sub-family of structurally related compounds to AXKO-0010. We found that 63 out of 75 related compounds showed highly potent LDHB inhibitory activities while maintaining selectivity. Of these, AXKO-0046 showed the greatest potency for LDHB inhibition (IC_{50} = 42 nM).

Next, the mechanism of LDHB inhibition of AXKO-0046 was evaluated using substrate-competition assay. AXKO-0046 was tested at five different NADH and pyruvate concentrations. Surprisingly, increasing the amount of pyruvate and NADH correlated with increased AXKO-0046 inhibition activity, thus suggesting an uncompetitive inhibitory mechanism with respect to both NADH and pyruvate. This indicates that this compound likely binds the enzyme–substrate complex. Several other selective LDHA inhibitors, such as galloflavin, oxamate, diacid-malonate scaffolds, and quinoline 3-sulphonamides have been described; however, these compounds are substrate-competitive inhibitors owing to the interaction with the catalytic site[9, 22, 23, 24].

Notably, the NADH concentration in cancer cells is generally elevated and has been reported to range from 168 to 870 μM[25]. The reported data suggest that LDHA likely binds to NADH in cells. As a result, a competitive inhibitor with NADH might generally yield poor cellular activity[24]. Because AXKO-0046 is uncompetitive with respect to both NADH and pyruvate, we hypothesise that increased intracellular NADH and pyruvate levels would increase LDHB inhibition, unlike competitive behaviour. Structural studies would provide further insights to understand the binding site of AXKO-0046, as well as the interaction residues of the LDHB protein for compound design to inhibit LDHB activity.

The crystal structure of the quaternary complex with NADH, oxamate, and AXKO-0046 revealed that AXKO-0046 is an allosteric inhibitor distant from the catalytic site. The binding mode of AXKO-0046 was spatially correlated with SAR studies to rationalise critical functional groups. The indole ring occupies a shallow pocket between the dimer interface, and its NH group forms a hydrogen bond with the main chain oxygen of Ser203. The reduced LDHB inhibitory activity of the N-Me derivative (AXKO-0067) is attributed to the disappearance of the interaction. In addition, two amino groups of AXKO-0046 can form hydrogen bonds with Glu214 at symmetry-related location of the tetramer. The methylated derivatives of AXKO-0046 (AXKO-0060, AXKO-0077, and AXKO-0058) also showed reduced LDHB inhibitory activity, which would be due to the attenuation of the interactions. The glutamic acid of LDHB (Glu214) is replaced by threonine in LDHA (Supplementary Figure S8 and S9). Near the AXKO-0046 binding site, two lysine residues of LDHB (Lys308 and Lys310) are also substituted by threonine in LDHA. The selectivity of AXKO-0046 may thus be attributed to these amino acid differences.

Loading [MathJax]/jax/output/CommonHTML/fonts/TeX/fontdata.js

There are two binding sites in the tetramer that are located at the interface of two dimers. In bacterial LDH enzymes, the allosteric site of the activator, fructose 1,6-bisphosphate (FBP), is well-characterised for the regulation of enzymatic activity[26]. The FBP binding site is also located at the dimer interface but is structurally distinct from the binding site of AXKO-0046. Moreover, the regulatory mechanism of bacterial LDHs is not applicable to the inhibitory mechanism of AXKO-0046 against LDHA and LDHB. Based on the crystal structures, the allosteric transition by the activator within two subunits is not required for the LDHB activity. Recently, machilin A (MA) has been reported to bind to LDHA in an interfacial allosteric site close to the FBP binding site[27]. However, its binding conformation of MA remains controversial because steric clashes of the protein–ligand interactions have been observed. Overall, we concluded that the binding site of AXKO-0046 is a unique allosteric binding site of a selective LDHB inhibitor.

The structural comparison between our quaternary and binary complexes revealed that the active-site loop, referred to as the substrate-specificity loop, exhibits closed and open conformations during the binding and release of substrates, respectively (Supplementary Fig. 7). The active-site loop of the closed conformation interacts with the C-terminal helix through hydrophobic interactions among Leu108, Thr323, Leu324, and Ile327 (Fig. 6). The substantial conformational changes in the active-site loop, accompanied by the conformational shift in the C-terminal helix, are associated with the binding site of AXKO-0046. These results suggest that substrate binding mediates the forging of the allosteric binding site and facilitates the specific binding of AXKO-0046. Consequently, the AXKO-0046 binding interferes with the machinery of the enzyme, although the substrate is bound. This structural observation is consistent with the results of substrate-competition assay suggesting that the inhibitory mechanism of AXKO-0046 is uncompetitive.

In conclusion, the LDHB assay we developed to monitor its activity has numerous advantages over current assay methods. Particularly, our method is continuous, non-radioactive, irreversible, robust, and versatile. In this study, we showed that AXKO-0046 acts as a potent specific inhibitor of LDHB in an uncompetitive manner. Thus, AXKO-0046 can be helpful in the exploration of molecular probes to elucidate the biological functions and therapeutic relevance of LDHB as a drug target. The compound can also be a useful tool for elucidating cancer metabolism. Furthermore, this series may be necessary lead optimization to enable *in vivo* evaluation at exposure levels that are not generally toxic. Our findings provide a promising starting point for development of drugs to treat LDHB-related diseases.

Methods

Materials

Recombinant human LDHA and LDHB were purchased from R&D (Minneapolis, MN, USA). NAD^+ was purchased from MP Biomedicals (Santa Ana, CA, USA). DTT, NaCl, and Triton X-100 were obtained from Sigma–Aldrich (St. Louis, MO, USA). Dihexylammonium acetate (DHAA) was obtained from Tokyo Kasei Kogyo (Tokyo, Japan). NADH, Pyruvate, bovine serum albumin (BSA), and other reagents were purchased

Loading [MathJax]/jax/output/CommonHTML/fonts/TeX/fontdata.js

AXKO-0046 was synthesised by the Takeda Pharmaceutical Co. Ltd., whereas AXKO-0058, AXKO-0060, AXKO-0067, and AXKO-0077 were synthesised by Axcelead Drug Discovery Partners, Inc.

LDHB and LDHA Assays for Primary Screening

We performed a screening campaign for compounds (final concentration: 10 μM) within pooled libraries consisting of more than 345,000 compounds. Each compound in DMSO (1 mM) was dispensed to 384-well V base plates (100 nl per well) using an Echo 555 acoustic dispenser (Labcyte, Sunnyvale, CA, USA). LDHB (5 μl was diluted in the assay buffer (20 mM Tris at pH 7.5, containing 2 mM DTT, 0.005% Triton X100, and 0.005% BSA) and dispensed to the assay plates (final concentration: 0.25 nM). The plates were centrifuged (200×g for 1 min), incubated at room temperature for 30 min, and added with 5 μl of NADH and pyruvate in the assay buffer (final concentration: 75 μM). After incubation for 30 min at room temperature, the plates were added with acetonitrile (10 μl) and water (50 μl) to quench the reaction. All additions were performed using a Multidrop Combi (Thermo Fisher Scientific, Waltham, MA, USA). Assay plates were sealed and centrifuged (2,700×g for 10 min) prior to storage at −20 °C.

The conditions for LDHA assay were as described above, except for substrate concentrations, i.e., 400 μM pyruvate and 100 μM NADH). These concentrations were chosen based on fitting to the Michaelis–Menten model with Km value (Supplementary Figure S2).

High-Throughput Mass Spectrometry Assay

For RapidFire mass assay (Agilent, Wakefield, MA, USA), the enzyme reaction solution (5 μl) was aspirated directly from the quenched assay plates and loaded onto a C8 solid-phase extraction cartridge (Agilent) with a mobile phase of water containing DHAA (5 mM) for 2,500 ms at a flow rate of 1.25 ml/min. Then, the analytes were coeluted into the mass spectrometer using water:acetonitrile:acetone (2:1:1) containing ammonium acetate (5 mM) for 5,000 ms at a flow rate of 1.0 ml/min. NADH and NAD^+ were detected using multiple reaction monitoring with QI/Q3 transitions at m/z 664.2 to 397.0 and m/z 662.1 to 540.1, respectively, on Sciex API4000 triple quadrupole mass spectrometer (Applied Biosystems, Foster City, CA, USA) in the negative electrospray ionization mode. Extracted ion chromatograms for each transition were integrated and processed using RapidFire Integrator (Agilent). The data for each well were normalised using the monitoring product conversion with the ratio of $AUC_{product}$ / ($AUC_{product}$+ $AUC_{substrate}$).

To determine the compound activities, percent inhibition data normalised to 0% (DMSO only) and 100% inhibition (no-enzyme control) wells were calculated. Data analysis was performed using Tibco Spotfire (Boston, MA, USA) packages.

Substrate-Competition Assay

To evaluate the mechanism of inhibition of the selected compounds, their initial reaction velocities were measured using 5 concentrations of NADH or pyruvate (10, 30, 50, 100, and 200 μM) incubated with the

Loading [MathJax]/jax/output/CommonHTML/fonts/TeX/fontdata.js

100 μM pyruvate for NADH titration or 100 μM NADH for pyruvate titration. Then, the solution of 7 concentrations of AXKO-0046 (0.00001, 0.0001, 0.001, 0.01, 0.1, 1, 10, and 100 μM) with LDHB of 0.25 nM were added. The enzymatic reactions were performed at room temperature for 15 min and conducted in triplicate. At each inhibitor concentration, the dependence of the initial reaction velocities on substrate concentration was fitted to nonlinear fits of Michaelis–Menten model to obtain the Km and Vmax values using GraphPad Prism. Lineweaver–Burk plot was generated by superimposing the data of 1/ [velocity] and 1/ [substrate] and the line corresponding to the Michaelis–Menten nonlinear fits.

Protein preparation for structural analysis

Human LDHB (Ala2–Leu334) (NCBI Reference Sequence: NM_001174097.2) DNA was synthesised and ligated into a pET21a vector (Merck Millipore, Darmstadt, Germany) with a N-terminal His-Avi tag, followed by the cleavage site of TEV protease using VectorBuilder (Chicago, IL, USA). The expression plasmid was transfected into *E. coli* BL21 (DE3) (Nippon Gene, Toyama, Japan), and the cells were grown in Lysogeny broth (LB) medium containing ampicillin (100 mg ml^{-1}). Protein expression was induced with Isopropyl β-d-1-thiogalactopyranoside (IPTG) (0.2 mM) and cultured for 16 h at 16 °C. Harvested cells were lysed using sonication in lysis buffer (50 mM Tris, pH 8.0), NaCl (150 mM), nuclease (5 U mL^{-1}) and centrifuged at 15,000×g for 10 min at 4 °C. The clarified supernatant was loaded onto Ni-NTA Cartridge (FUJIFILM Wako, Osaka, Japan), and the eluted fraction was purified on HiLoad 26/60 Superdex 200 pg column (GE Healthcare, Piscataway, NJ, USA). The His–Avi tag was digested using TEV protease (Sigma-Aldrich, St. Louis, MO, USA), and the digested solution was subsequently passed through a Ni-NTA column to remove TEV protease and the uncleaved protein.

The protein was further purified using anion-exchange chromatography (monoQ, GE Healthcare) with a linear gradient of NaCl. All purification steps were assessed using SDS–PAGE and Coomassie Blue staining (Sigma-Aldrich, St. Louis, MO, USA). The final yield of protein was 46 mg for every 1 litre of culture. For crystallization, the purified protein was buffer-exchanged to the final buffer (50 mM Tris, pH 7.6 with 150 mM NaCl), concentrated (20 mg ml^{-1}) using ultrafiltration (AMICON-ULTRA 10K, Millipore, Bedford, MA, USA), and stored at −80°C.

X-ray crystallography

The complexes of LDHB with NADH or NADH, oxamate, and AXKO-0046 were generated by incubating 3-fold molar excesses of ligands on ice for 2–3 h before crystallization experiments. Both complexes were crystallised from a reservoir solution containing HEPES (0.1 M, pH 7.5), potassium formate or ammonium acetate (0.2 M), and PEG 3350 (20% v/v) at 20°C via the sitting-drop vapour diffusion method. Prior to data collection, crystals were immersed in the reservoir solution containing ethylene glycol (30%) as a cryoprotectant and flash-frozen in liquid nitrogen. Diffraction data were collected from a single crystal using the DECTRIS Pilatus3-S6M PAD detector (Baden-Daettwil, Switzerland) with a BL45XU beamline (SPring-8, Hyogo, Japan) under a 100 K nitrogen cryostream. The diffraction data were reduced and scaled using HKL 2000[28]

Loading [MathJax]/jax/output/CommonHTML/fonts/TeX/fontdata.js

The structure was solved according to the molecular replacement method using Phaser[29] from the CCP4 software suite[30] and the LDHB structure (PDB code 1I0Z[18]) as a search model. Refinement was performed using REFMAC5[31] with individual isotropic restrained B factors. Some data (5%) were set aside for cross-validation before refinement, and progress was monitored using R_{free}. For TLS refinement, the tetramer of the protein and ligands was set as a single rigid body[32]. Interactive model building was performed using COOT[33]. The final models were validated using Molprobity[34]. All graphical figures were generated using PyMOL (Schrödinger LLC, Cambridge, MA, USA). Crystallographic processing and refinement statistics are summarised in Supplementary Table S1.

Data Analysis

For the kinetic parameters, the initial rates of LDH activity were determined by incubating LDHA or LDHB with various concentrations of NADH and pyruvate in the assay buffer at room temperature. The reaction product was measured using RapidFire mass assay. To estimate the Km and Vmax values, the initial rates were fit to the Michaelis–Menten equation. IC_{50} and Hill slope calculation and curve fitting using four-parameter fits were performed using GraphPad Prism v6.07 (GraphPad Software, San Diego, CA) or XLfit (IDBS, Guildford, UK) with nonlinear regression analysis, wherein the IC_{50} value equals the concentration at which the inflection point of the fitted model is reached. The quality and robustness of the screening campaign were determined by analysing the Z’ factor.

Declarations

Acknowledgements

The authors thank the following colleagues at the Axcelead Drug Discovery Partners for their valuable support: Ms. Mai Okada for the evaluation of the compounds, Mr. Takamitsu Maru and Mr. Hideyuki Oki for the biophysical assays. We also thank Dr. Junji Matsui, for his supervision and valuable suggestions.

Author contributions

T.S. conceptualized and coordinated the study. A.N., S.K., and T.K. conceived and designed the experiments. S. Shibata screened the compound libraries, performed inhibition studies, and wrote the manuscript. S. Sogabe performed protein crystallization, analysed the diffraction data, and wrote the manuscript. N.T. and T.F. designed and synthesized the chemical compound. All authors critically revised the content and approved the final version for submission.

Competing Interests

The authors declare no competing interests.

Data Availability

Loading [MathJax]/jax/output/CommonHTML/fonts/TeX/fontdata.js

The atomic coordinates and structure factors have been deposited in the Protein Data Bank with the primary accession codes 7DBJ and 7DBK. The data that support the findings of this study are available from the corresponding authors upon reasonable request.

References

1. Hsu, P. P. & Sabatini, D. M. Cancer cell metabolism: Warburg and beyond. *Cell* **134**, 703–707 (2008).
2. Warburg, O. On the origin of cancer cells. *Science* **123**, 309–314 (1956).
3. Vander Heiden, M. G., Cantley, L. C. & Thompson, C. B. Understanding the Warburg effect: the metabolic requirements of cell proliferation. *Science* **324**, 1029–1033 (2009).
4. Valvona, C. J., Fillmore, H. L., Nunn, P. B. & Pilkington, G. J. The regulation and function of lactate dehydrogenase A: therapeutic potential in brain tumor. *Brain Pathol.* **26**, 3–17 (2016).
5. Kolev, Y., Uetake, H., Takagi, Y. & Sugihara, K. Lactate dehydrogenase-5 (LDH-5) expression in human gastric cancer: association with hypoxia-inducible factor (HIF-1alpha) pathway, angiogenic factors production and poor prognosis. *Ann. Surg. Oncol.* **15**, 2336–2344 (2008).
6. Koukourakis, M. I., *et al*. Lactate dehydrogenase-5 (LDH-5) overexpression in non-small-cell lung cancer tissues is linked to tumour hypoxia, angiogenic factor production and poor prognosis. *Br. J. Cancer* **89**, 877–885 (2003).
7. Le, A., *et al*. Inhibition of lactate dehydrogenase A induces oxidative stress and inhibits tumor progression. *Proc. Natl Acad. Sci. U. S. A.* **107**, 2037–2042 (2010).
8. Sheng, S. L., *et al*. Knockdown of lactate dehydrogenase A suppresses tumor growth and metastasis of human hepatocellular carcinoma. *FEBS Journal* **279**, 3898–3910 (2012).
9. Billiard, J., *et al*. Quinoline 3-sulfonamides inhibit lactate dehydrogenase A and reverse aerobic glycolysis in cancer cells. *Cancer Metab.* **1**, 19 (2013).
10. McCleland, M. L., *et al*. Lactate dehydrogenase B is required for the growth of KRAS-dependent lung adenocarcinomas. *Clin. Cancer Res.* **19**, 773–784 (2013).
11. McCleland, M. L., *et al*. An integrated genomic screen identifies LDHB as an essential gene for triple-negative breast cancer. *Cancer Res.* **72**, 5812–5823 (2012).
12. Satoh, K., *et al*. Global metabolic reprogramming of colorectal cancer occurs at adenoma stage and is induced by MYC. *Proc. Natl Acad. Sci. U. S. A.* 114, E7697–E7706 (2017).
13. Brisson, L., *et al*. Lactate dehydrogenase B controls lysosome activity and autophagy in cancer. *Cancer Cell* **30**, 418–431 (2016).
14. White, E. Deconvoluting the context-dependent role for autophagy in cancer. *Nat. Rev. Cancer* **12**, 401–410 (2012).
15. LeVan, K. M. & Goldberg, E. Properties of human testis-specific lactate dehydrogenase expressed from *Escherichia coli*. *Biochem. J.* **273**, 587–592 (1991).
16. Matoba, Y., *et al*. An alternative allosteric regulation mechanism of an acidophilic l-lactate [illegible] *FEBS Open Bio* **4**, 834–847 (2014).

Loading [MathJax]/jax/output/CommonHTML/fonts/TeX/fontdata.js

17. Pirrung, M. C., *et al*. Methyl scanning: total synthesis of demethylasterriquinone B1 and derivatives for identification of sites of interaction with and isolation of its receptor(s). *J. Am. Chem. Soc.* **127**, 4609–4624 (2005).
18. Read, J. A., Winter, V. J., Eszes, C. M., Sessions, R. B. & Brady, R. L. Structural basis for altered activity of M- and H-isozyme forms of human lactate dehydrogenase. *Proteins* **43**, 175–185 (2001).
19. Thabault, L., *et al*. Interrogating the lactate dehydrogenase tetramerization site using (stapled) peptides. *J. Med. Chem.* **63**, 4628–4643 (2020).
20. Granchi, C., *et al*. Discovery of N-hydroxyindole-based inhibitors of human lactate dehydrogenase isoform A (LDH-A) as starvation agents against cancer cells. *J. Med. Chem.* **54**, 1599–1612 (2011).
21. Vanderporten, E., *et al*. Label. Label-free high-throughput assays to screen and characterize novel lactate dehydrogenase inhibitors. *Anal. Biochem.* **441**, 115–122 (2013).
22. Zhai, X., Yang, Y., Wan, J., Zhu, R. & Wu, Y. Inhibition of LDH-A by oxamate induces G2/M arrest, apoptosis and increases radiosensitivity in nasopharyngeal carcinoma cells. *Oncol. Rep.* **30**, 2983–2991 (2013).
23. Manerba, M., *et al*. Galloflavin (CAS 568-80-9): a novel inhibitor of lactate dehydrogenase. *ChemMedChem* **7**, 311–317 (2012).
24. Ward, R. A., *et al*. Design and synthesis of novel lactate dehydrogenase A inhibitors by fragment-based lead generation. *J. Med. Chem.* **55**, 3285–3306 (2012).
25. Yu, Q. & Heikal, A. A. Two-photon autofluorescence dynamics imaging reveals sensitivity of intracellular NADH concentration and conformation to cell physiology at the single-cell level. *J. Photochem. Photobiol. B Biol.* **95**, 46–57 (2009).
26. Iwata, S., Kamata, K., Yoshida, S., Minowa, T. & Ohta, T. T and R states in the crystals of bacterial L-lactate dehydrogenase reveal the mechanism for allosteric control. *Nat. Struct. Biol.* **1**, 176–185 (1994).
27. Chung, T. W., *et al*. Machilin A inhibits tumor growth and macrophage M2 polarization through the reduction of lactic acid. *Cancers* **11** (2019).
28. Otwinowski, Z. & Minor, W. Processing of X-ray diffraction data collected in oscillation mode. *Methods Enzymol.* **276**, 307–326 (1997).
29. McCoy, A. J., *et al*. Phaser crystallographic software. *J. Appl. Crystallogr.* **40**, 658–674 (2007).
30. Winn, M. D., *et al*. Overview of the CCP4 suite and current developments. *Acta Crystallogr. D Biol. Crystallogr.* **67**, 235–242 (2011).
31. Murshudov, G. N., Vagin, A. A. & Dodson, E. J. Refinement of macromolecular structures by the maximum-likelihood method. *Acta Crystallogr. D Biol. Crystallogr.* **53**, 240–255 (1997).
32. Winn, M. D., Isupov, M. N. & Murshudov, G. N. Use of TLS parameters to model anisotropic displacements in macromolecular refinement. *Acta Crystallogr. D Biol. Crystallogr.* **57**, 122–133 (2001).

Loading [MathJax]/jax/output/CommonHTML/fonts/TeX/fontdata.js

33. Emsley, P., Lohkamp, B., Scott, W. G. & Cowtan, K. Features and development of coot. *Acta Crystallogr. D Biol. Crystallogr.* **66**, 486–501 (2010).

34. Chen, V. B., *et al.* MolProbity: all-atom structure validation for macromolecular crystallography. *Acta Crystallogr. D Biol. Crystallogr.* **66**, 12–21 (2010).

Figures

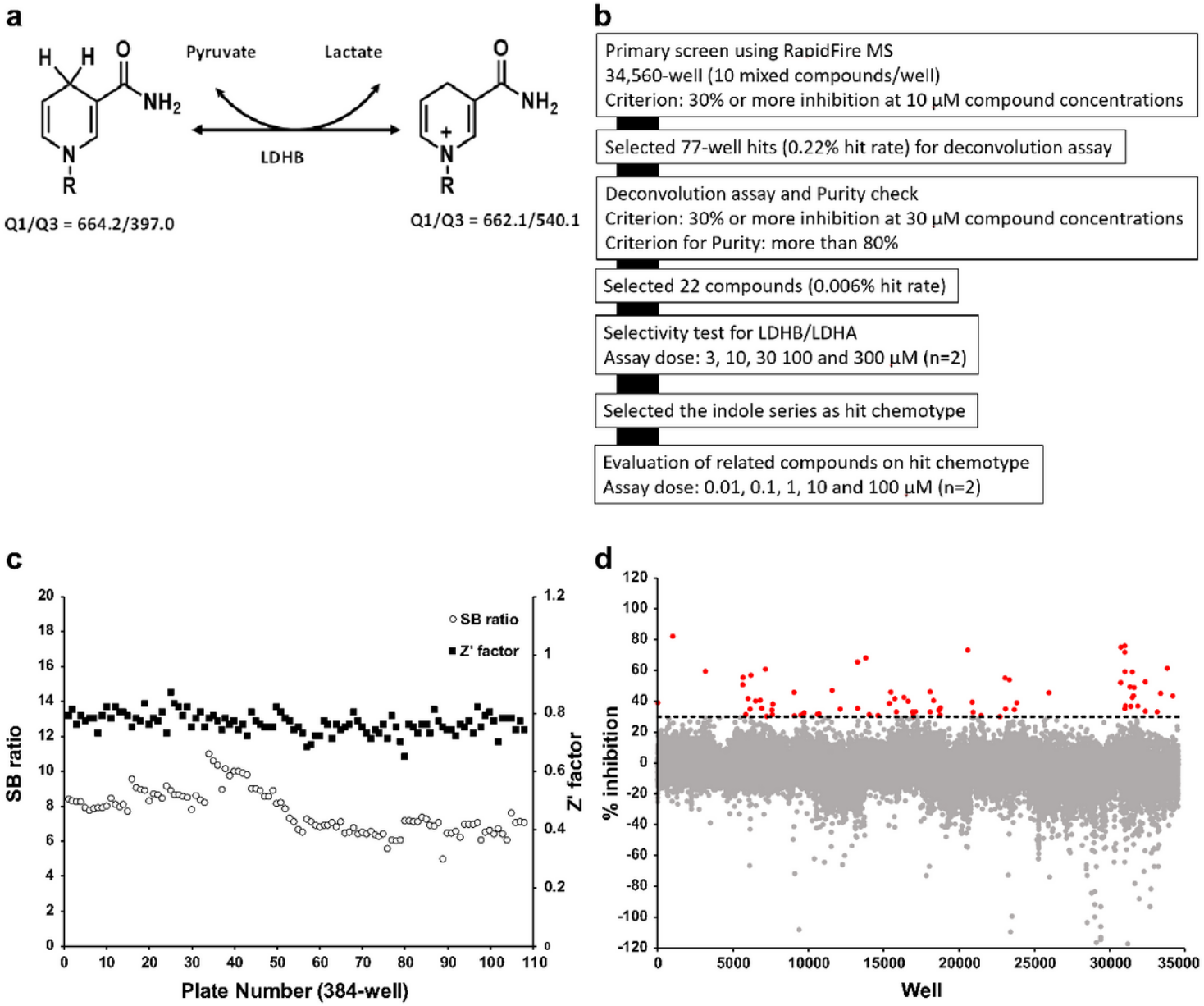

Figure 1

Primary screening for inhibitors of lactate dehydrogenase B (LDHB). a LDHB-catalyzed reaction scheme. NADH and NAD+ were detected using mass spectrometry with their respective MRM shown. b Screening cascade and results of primary screening. The high-throughput screening cascade consisted of the acterization. A diverse library of small

Loading [MathJax]/jax/output/CommonHTML/fonts/TeX/fontdata.js

compounds from Axcelead at 10 μM was screened against LDHB. c SB ratio (open circles) and Z'-factor values (filled squares) of the overall primary screening. d Scatterplots of primary screening data and selection of hit wells exhibiting >30% inhibition activity (red circles).

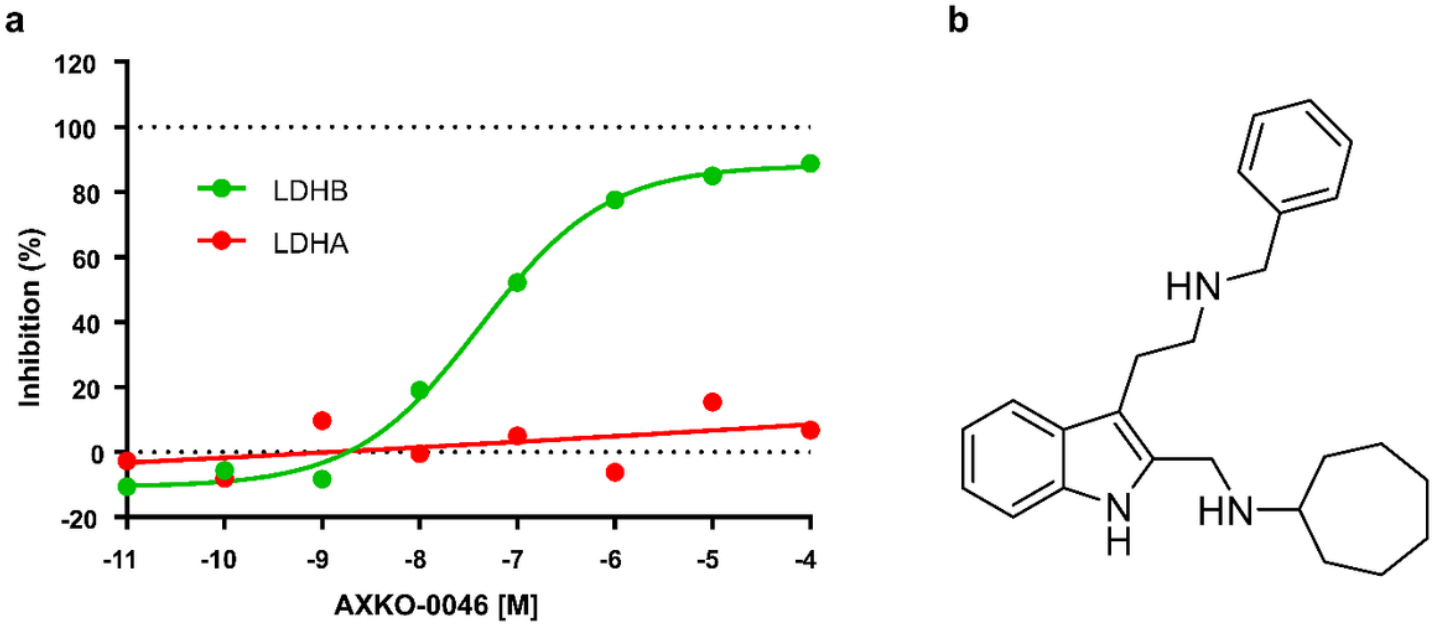

Figure 2

Concentration response curve and the structure of AXKO-0046. a Concentration response curves and IC50 values of AXKO-0046. AXKO-0046 selectively inhibited LDHB (green circles) but did not inhibit LDHA (red circles). IC50 for LDHB was 42 nM. The curves were fitted to the standard four-parameter logistic equation. b Structure of AXKO-0046. Data shown are mean (n=2).

Loading [MathJax]/jax/output/CommonHTML/fonts/TeX/fontdata.js

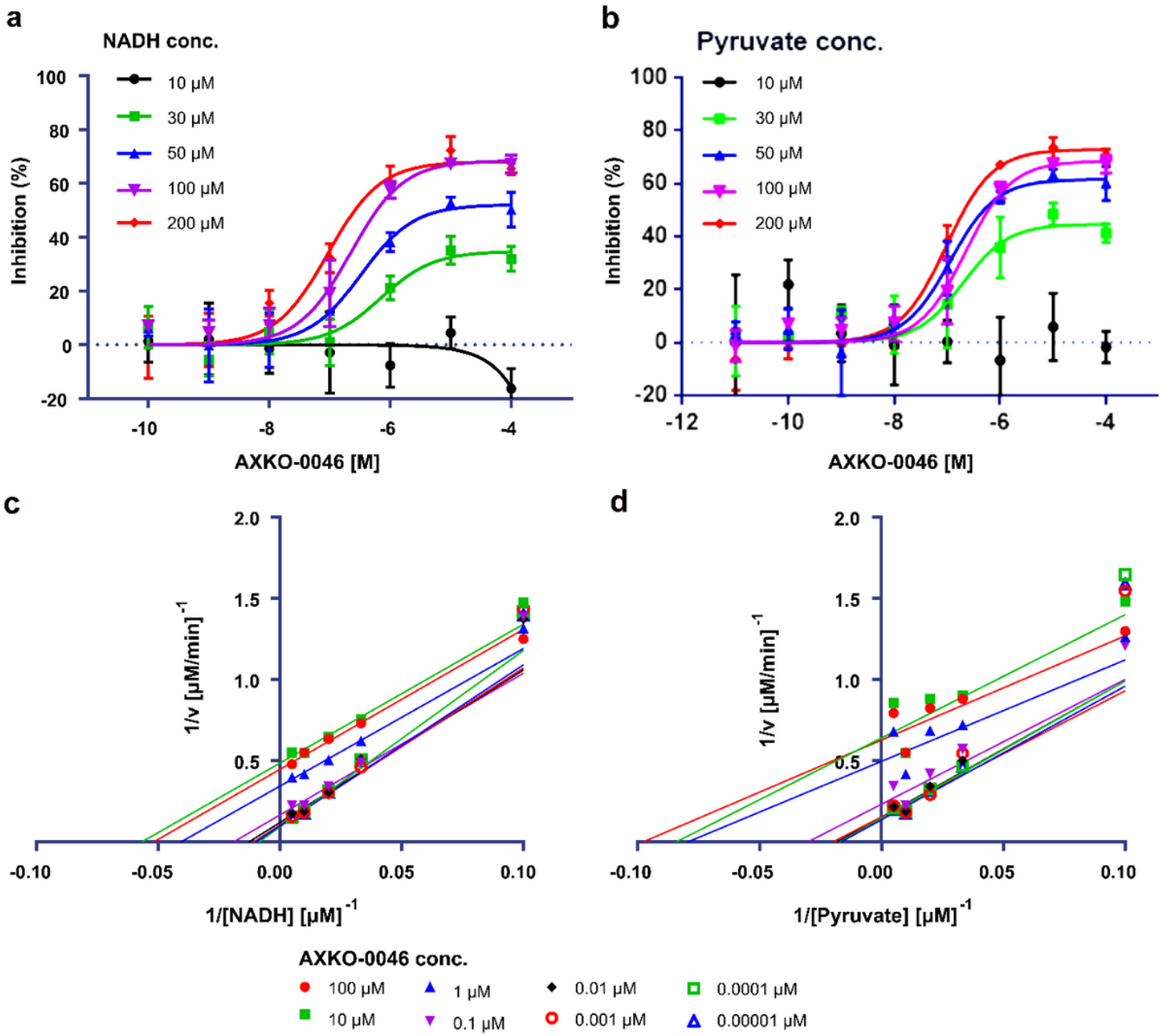

Figure 3

Biochemical characterization of AXKO-0046. a, b LDHB inhibition by AXKO0046 was studied using varying concentrations of a, NADH and b, pyruvate. IC50 values of AXKO-0046 decreased with increasing pyruvate and NADH concentrations. Data shown are mean ± standard deviation (SD) (n=3). c, d Lineweaver-Burk plots of the kinetic data in Table 1 with nonlinear regression analysis of c, NADH and d, pyruvate.

Loading [MathJax]/jax/output/CommonHTML/fonts/TeX/fontdata.js

	R^1	R^2	R^3	IC_{50} (μM)
AXKO-0046	H	H	H	0.042
AXKO-0067	Me	H	H	>100
AXKO-0060	H	Me	H	0.26
AXKO-0077	H	H	Me	6.3
AXKO-0058	H	Me	Me	8.3

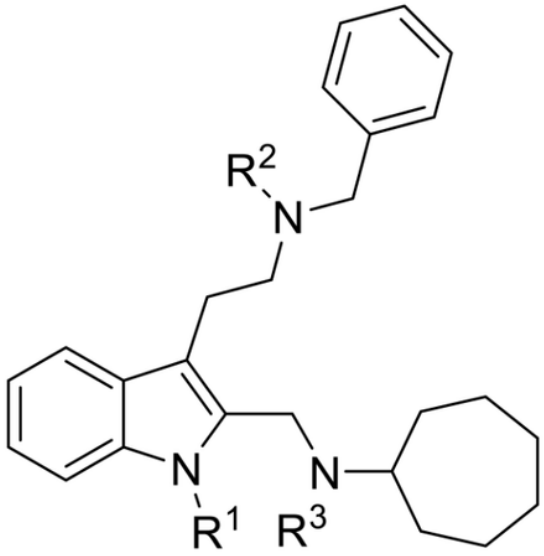

Figure 4

Chemical structure of AXKO-0046 derivatives and their IC50 values.

Loading [MathJax]/jax/output/CommonHTML/fonts/TeX/fontdata.js

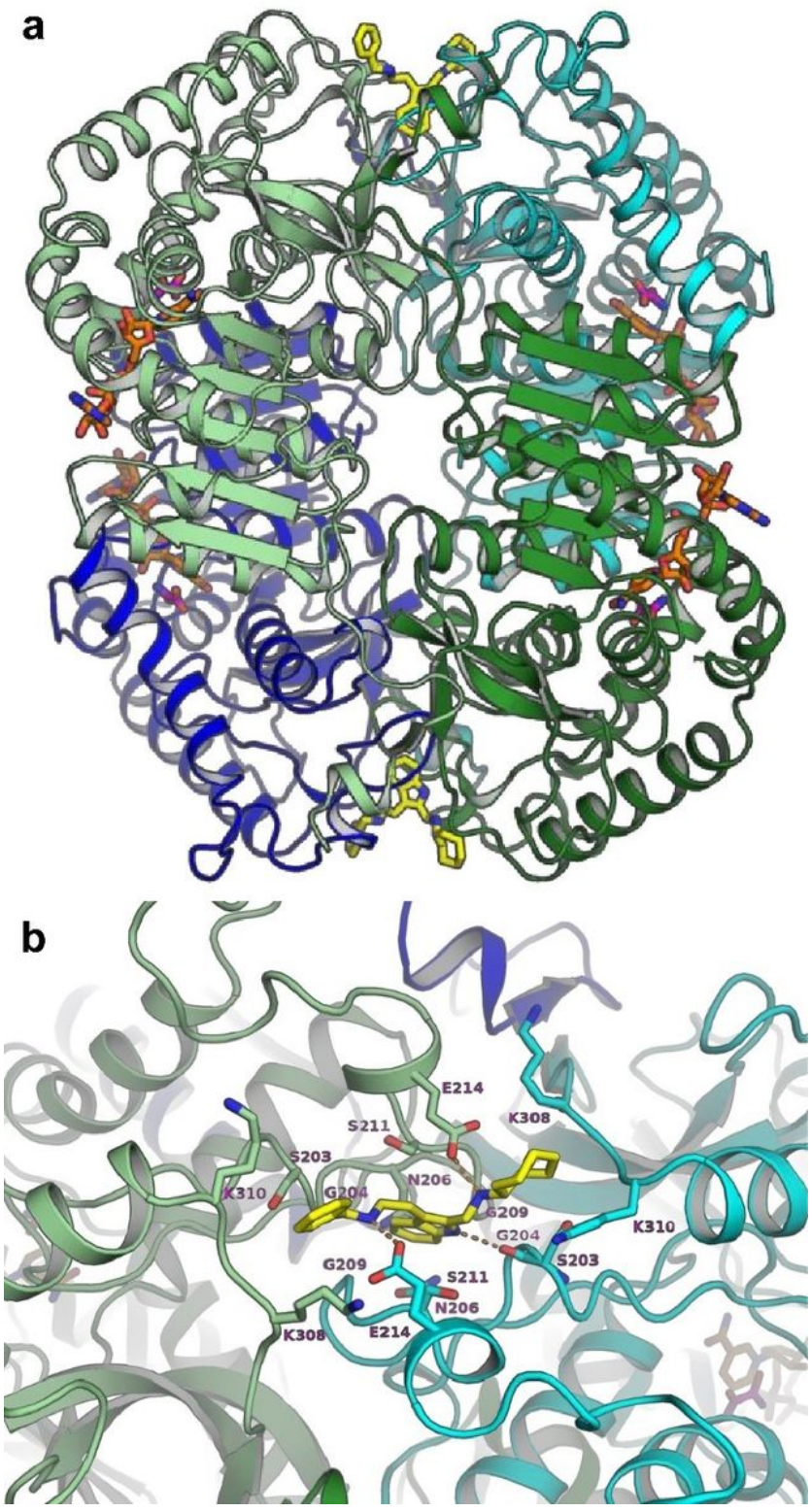

Figure 5

Crystal structure of the quaternary LDHB/NADH/oxamate/AXKO-0046 complex. a Ribbon diagram. b Close-up view of the binding site of AXKO-0046. Each monomer of the tetramers is shown in lime, forest, cyan, and blue. NADH, oxamate, and AXKO-0046 are depicted as stick models in orange, magenta, and yellow, respectively.

Loading [MathJax]/jax/output/CommonHTML/fonts/TeX/fontdata.js

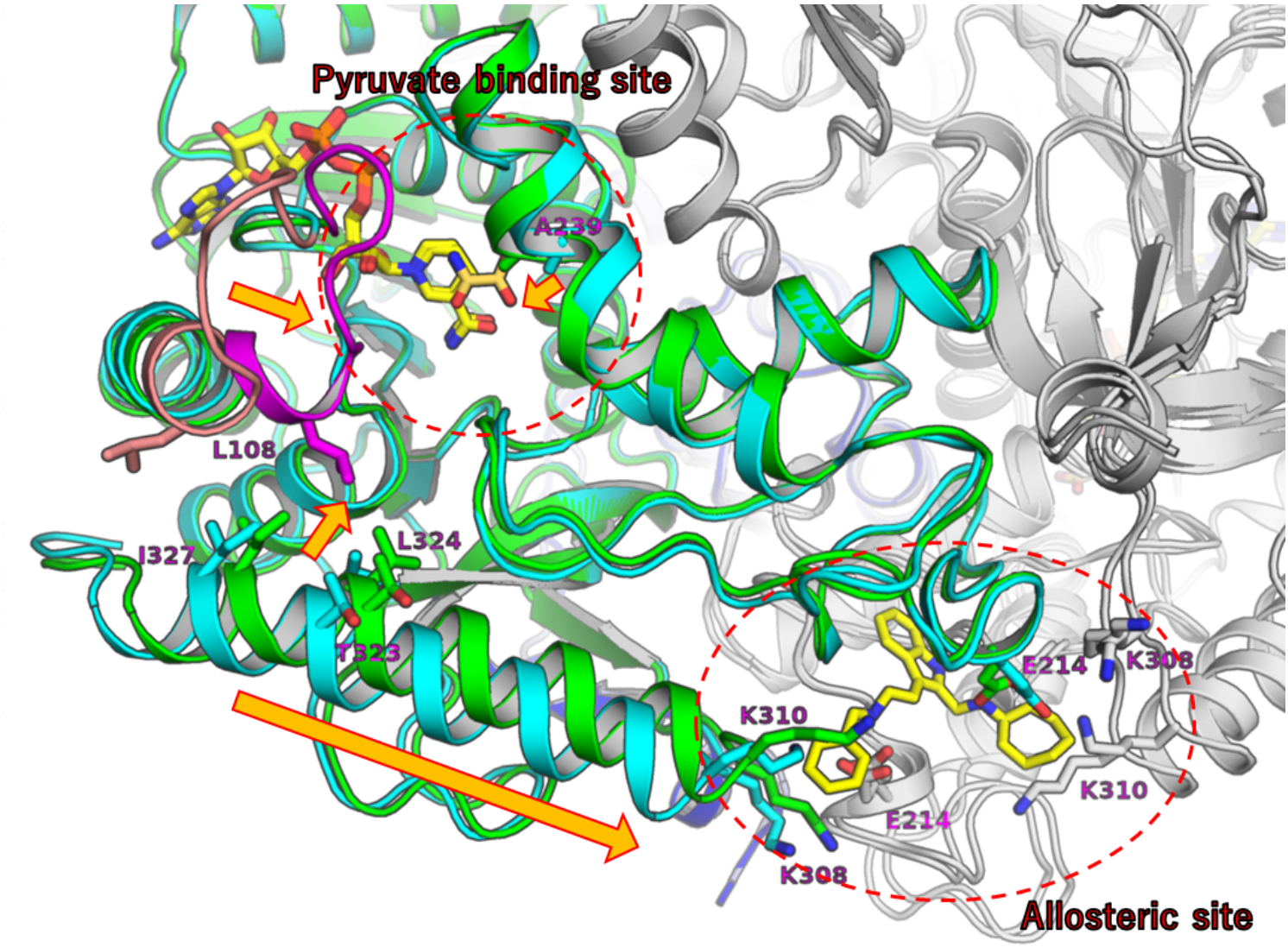

Figure 6

Superposition of the LDHB/NADH/oxamate/AXKO-0046 complex (green or magenta) with the LDHB/NADH complex (cyan or salmon). For clarity, one monomer of each tetramer is coloured, whereas others are in grey. NADH, oxamate, and AXKO-0046 are depicted as stick models in yellow, yellow-orange, and yellow, respectively. Key Side chains of key residues are also depicted as stick models and labelled. The active site and allosteric site are highlighted in red dot circles. Structural rearrangements by substrate binding are shown in orange arrows.

Supplementary Files

This is a list of supplementary files associated with this preprint. Click to download.

- supplementaryinformation.pdf

Loading [MathJax]/jax/output/CommonHTML/fonts/TeX/fontdata.js